

Study on Three-Dimensional Hydro-Mechanical-Chemical Fully Coupled Model for Pollutant Transport of Composite Liners

Yang Jinzhu

Key Laboratory of Urban Security and Disaster Engineering, Ministry of Education, Beijing University of Technology, Beijing, China

Abstract: In complex construction environment, there are often holes in the composite gasket geomembrane, and it is easy to bend upward to form wrinkles. Holes and wrinkles are the key factors for pollutants to enter the underlying clay bedding, which will change its hydraulic and mechanical properties and dynamic coupling response. The three-dimensional multi-physical field fully coupled model which can describe the true state of geomembrane defects can accurately predict the migration law of pollutants inside the composite gasket, which is of great significance for the design and service performance evaluation of the composite gasket. Based on Biot consolidation theory and the mass conservation equation of pore fluid and pollutant, a three-dimensional hydro-mechanical-chemical (HMC) fully coupled pollutant transport model with membrane defects is established in this paper. The coupling model was numerically calculated using COMSOL Multiphysics software, and the coupling response laws of soil under two conditions with only holes and wrinkles were compared and analyzed. The results show that the existence of wrinkles can not only expand the pollutant leakage area, but also increase the negative pore water pressure and the depth of influence. Increasing the amount of soil settlement and rebound makes the pad appear uneven settlement; At the same time, it will greatly accelerate the migration rate of pollutants. Compared with the condition without wrinkle, the maximum negative pore water pressure and sedimentation amount in the initial stage increased by 80% and 50%, respectively, and the breakdown depth of pollutants increased by 97.6% when the simulation time was 50 years.

Keywords: Holes; Wrinkles; Three-dimensional

Hydro-mechanical-chemical Fully Coupled Model; Composite Liners

1. Introduce

The landfill liner system plays a crucial role in protecting the surrounding environment from pollution and secondary pollution [1-3]. The composite liner composed of geomembrane and compacted clay is a relatively common type of liner, among which the integrity of the geomembrane is the key to ensuring the barrier performance of this composite liner. However, due to factors such as the construction environment and construction quality, there are often a certain number of loopholes and wrinkles on the geomembrane, which accelerate the migration of pollutants in the composite liner and change the physicochemical properties and coupling responses of the underlying clay cushion layer. This seriously challenges the effective barrier of the composite liner against toxic and harmful substances [4, 5]. Meanwhile, the change in the spatial dimension will also affect the migration law of solute ions [6]. Therefore, establishing a multi-dimensional coupling model that can consider the defects of geomembranes and studying the migration and transformation laws of pollutants in defective composite liners have very important theoretical and practical significance for the design of composite liners and the assessment of their service life.

When studying the migration problem of pollutants in clay bedding layers, it is usually assumed that porous media are rigid materials, and on this basis, the mechanisms of pollutant adsorption, biodegradation and convection-diffusion are considered [7-10]. Due to the self-weight of solid waste, the clay liner will undergo mechanical consolidation, changing the inherent transport characteristics of the soil and affecting the migration and transformation laws of pollutants [2, 11-12]. Smith [13] proposed the theory of solute

transport in saturated deformable porous media. Qiu et al. [14] derived the analytical solution of the one-dimensional consolidation and migration coupling problem that can take into account the nonlinear compression and permeability characteristics of porous media. Xie et al. [15] established a one-dimensional mathematical model that could consider the coupling effects of consolidation, diffusion and degradation, and investigated the migration behavior of pollutants in GMB/CCL composite liners. With the maturity and improvement of the coupling theory, more and more studies have begun to focus on soil deformation caused by the presence of pollutants, namely chemical-permeable consolidation [12, 16-18]. Chemically-permeable consolidation can change the pore structure of the soil, increase the settlement of the soil, and affect the multi-physical field coupling response within the cushion layer. To explore the influence of chemical-osmotic consolidation on the migration process of pollutants, Zhang et al. [11] established a relatively complete water-mechanical-chemical coupling model, but this model was a one-dimensional one. To conform to engineering practice, Zhang et al. [19, 20] extended their one-dimensional coupling model to three dimensions.

Although the above-mentioned coupling model can well describe the migration law of pollutants when the leachate is in direct contact with the clay liner, for the composite liner system, a geomembrane with better sealing performance is often laid above the clay cushion layer, so that the clay liner does not come into direct contact with the leachate. Research has found that due to the construction environment and construction quality, geomembranes are inevitably damaged during the laying process. On-site data shows that despite strict control over construction quality, 70% of the geomembranes still have tearing conditions [21-24]. In addition, when installing geomembranes under conditions of high ambient temperature, the geomembranes will undergo expansion and deformation. When the expansion and deformation are constrained, the geomembranes will bend upward to form wrinkles [25]. There are a large number of wrinkles on the geomembrane. Affected by the compaction of the underlying clay cushion layer and the flatness of the surface, the coverage rate can reach 30%, and it will not disappear due to the self-weight of the upper garbage pile.

Furthermore, studies have shown that when the leakage frequency of geomembrane is 2.5-5 per hectare, approximately one leakage is located on the hydraulically connected folds [26, 27]. Zhan Liangtong et al. [28] conducted leakage detection on 11 landfills in China. The detection results revealed that the average leakage frequency on the geomembrane was approximately 24 per ha. Evidently, when studying the migration and transformation laws of pollutants within defective composite gaskets, it is necessary not only to consider the loopholes but also the combined influence of the loopholes and wrinkles. The one-dimensional coupling model only restricts the vertical transmission of solutes and fluids, and cannot accurately depict the real existence state of membrane defects, and is rather difficult to precisely describe the transport law of pollutants within the horizontal clay cushion layer. Therefore, it is urgently necessary to establish a three-dimensional multiphysics field fully coupled model that can consider membrane defects.

In this study, through the Biot consolidation theory, the mass conservation equation of pore fluid and pollutants, a three-dimensional water-mechanized (HMC) fully coupled pollutant transport model considering the defects of geomembranes was established. The established model can not only accurately depict the real existence state of membrane defects, but also take into account the dynamic changes of hydraulic and mechanical characteristic parameters of soil. Using the established fully coupled model and the finite element software COMSOL Multiphysics for numerical calculations, the influences of vulnerabilities and folds on the changes of pore water pressure within the soil mass, the settlement evolution of the soil mass, and the migration laws of pollutants were explored.

2. Coupling Model and Control Equation

2.1 Basic Assumptions

The movement of pore fluids and the transport of pollutants respectively satisfy Darcy's Law and Fick's Law; Instantaneous application of load; The soil mass is a saturated small-deformation elastomer; Solid particles are incompressible under external loads. Its chemical composition is inorganic and it does not undergo chemical reactions with clay particles.

2.2 Soil Deformation Control Equation

The Biot consolidation equation not only satisfies the soil equilibrium condition and the elastic stress-strain relationship, but also takes into account the fluid continuity condition. Among them, the three-dimensional equilibrium equation of the soil element can be written as

$$\begin{cases} \frac{\partial \sigma_{xx}}{\partial x} + \frac{\partial \sigma_{xy}}{\partial y} + \frac{\partial \sigma_{zx}}{\partial z} = 0 \\ \frac{\partial \sigma_{xy}}{\partial x} + \frac{\partial \sigma_{yy}}{\partial y} + \frac{\partial \sigma_{yz}}{\partial z} = 0 \\ \frac{\partial \sigma_{zx}}{\partial x} + \frac{\partial \sigma_{zy}}{\partial y} + \frac{\partial \sigma_{zz}}{\partial z} = -\gamma_{sat} \end{cases} \quad (1)$$

In the formula, σ_{ij} ($i, j=x, y, z$) is the total stress and γ_{sat} sat is the saturation density.

According to the principle of effective stress, formula (1) can be written as

$$\begin{cases} \frac{\partial \sigma'_{xx}}{\partial x} + \frac{\partial \sigma'_{xy}}{\partial y} + \frac{\partial \sigma'_{zx}}{\partial z} + \frac{\partial u}{\partial x} = 0 \\ \frac{\partial \sigma'_{yx}}{\partial x} + \frac{\partial \sigma'_{yy}}{\partial y} + \frac{\partial \sigma'_{yz}}{\partial z} + \frac{\partial u}{\partial y} = 0 \\ \frac{\partial \sigma'_{zx}}{\partial x} + \frac{\partial \sigma'_{zy}}{\partial y} + \frac{\partial \sigma'_{zz}}{\partial z} + \frac{\partial u}{\partial z} = -\gamma' \end{cases} \quad (2)$$

In the formula, σ'_{ij} represents the effective stress and γ' is the effective specific gravity of pore water.

In isotropic linear porous elastic media, the

$$\begin{cases} -G\nabla^2 w_x - \frac{G}{1-2\nu} \frac{\partial}{\partial x} \left(\frac{\partial w_x}{\partial x} + \frac{\partial w_y}{\partial y} + \frac{\partial w_z}{\partial z} \right) - \alpha_c \frac{E}{1-2\nu} \frac{\partial c}{\partial x} + \frac{\partial u}{\partial x} = 0 \\ -G\nabla^2 w_y - \frac{G}{1-2\nu} \frac{\partial}{\partial y} \left(\frac{\partial w_x}{\partial x} + \frac{\partial w_y}{\partial y} + \frac{\partial w_z}{\partial z} \right) - \alpha_c \frac{E}{1-2\nu} \frac{\partial c}{\partial y} + \frac{\partial u}{\partial y} = 0 \\ -G\nabla^2 w_z - \frac{G}{1-2\nu} \frac{\partial}{\partial z} \left(\frac{\partial w_x}{\partial x} + \frac{\partial w_y}{\partial y} + \frac{\partial w_z}{\partial z} \right) - \alpha_c \frac{E}{1-2\nu} \frac{\partial c}{\partial z} + \frac{\partial u}{\partial z} = \gamma' \end{cases} \quad (5)$$

In the formula, ∇^2 is the Laplace operator.

2.3 Pore Water Flow Control Equation

The pore water continuity equation can be expressed as

$$\frac{\partial(n\rho_f)}{\partial t} + \nabla \cdot (n\rho_f \mathbf{q}_f) = 0 \quad (6)$$

In the formula: n represents porosity, ρ_f represents the density of the pore fluid, and \mathbf{q}_f represents the permeation velocity of the pore fluid.

When it is assumed that the pore fluid is incompressible, formula (6) can be simplified to

$$\frac{\partial n}{\partial t} + \nabla \cdot (n\mathbf{q}_f) = 0 \quad (7)$$

constitutive relationship of effective stress σ'_{ij} , strain ε_{ij} and chemical concentration changes can be expressed as [6, 20]

$$\begin{cases} \sigma'_{xx} = 2G \left(\frac{\nu}{1-2\nu} \varepsilon_v + \varepsilon_{xx} \right) - \alpha_c \frac{E}{1-2\nu} (c - c_s) \\ \sigma'_{yy} = 2G \left(\frac{\nu}{1-2\nu} \varepsilon_v + \varepsilon_{yy} \right) - \alpha_c \frac{E}{1-2\nu} (c - c_s) \\ \sigma'_{zz} = 2G \left(\frac{\nu}{1-2\nu} \varepsilon_v + \varepsilon_{zz} \right) - \alpha_c \frac{E}{1-2\nu} (c - c_s); \\ \sigma_{xy} = 2G\varepsilon_{xy}, \sigma_{zx} = 2G\varepsilon_{zx}, \sigma_{yz} = 2G\varepsilon_{yz} \end{cases} \quad (3)$$

In the formula: $\alpha_c = m_c(1-\nu)/(1+\nu)$, m_c is the coefficient of volume change caused by chemical concentration change, G is the shear modulus of soil, ν is the poisson ratio of soil, E represents the elastic modulus of the soil mass, c represents the concentration of pollutants within the soil mass, and c_s represents the concentration of pollutants in the leachate.

It can be known from the geometric equation

$$\begin{cases} \varepsilon_{xx} = -\frac{\partial w_x}{\partial x}, \varepsilon_{yz} = -\frac{1}{2} \left(\frac{\partial w_y}{\partial z} + \frac{\partial w_z}{\partial y} \right) \\ \varepsilon_{yy} = -\frac{\partial w_y}{\partial y}, \varepsilon_{xz} = -\frac{1}{2} \left(\frac{\partial w_z}{\partial x} + \frac{\partial w_x}{\partial z} \right) \\ \varepsilon_{zz} = -\frac{\partial w_z}{\partial z}, \varepsilon_{xy} = -\frac{1}{2} \left(\frac{\partial w_x}{\partial y} + \frac{\partial w_y}{\partial x} \right) \end{cases} \quad (4)$$

In the formula, w_x , w_y and w_z respectively represent the displacements of the soil framework in the x , y and z directions.

Substituting formula (3) and (4) into formula (2) will yield the soil deformation control equation

The porosity of soil under the combined action of mechanical load and pollutant concentration can be expressed as [29]

$$n = n_0 - \Delta n = n_0 + m_v \mu - m_c c \quad (8)$$

Substituting Formula (8) into Formula (7) yields the result

$$m_v \frac{\partial u}{\partial t} - m_c \frac{\partial c}{\partial t} + \nabla \cdot (n\mathbf{q}_f) = 0 \quad (9)$$

The pore water permeation velocity \mathbf{q}_f , the flow velocity \mathbf{q}_r of pore water relative to the soil skeleton and the soil particle velocity \mathbf{q}_s are satisfied

$$\mathbf{q}_f - \mathbf{q}_s = \mathbf{q}_r \quad (10)$$

The relationship between the flow velocity \mathbf{q}_r of pore water relative to the soil framework and the

generalized Darcy velocity \mathbf{q} , as well as the relationship between the soil particle velocity \mathbf{q}_s and the soil settlement, is satisfied

$$\mathbf{q}_r = \frac{1}{n}\mathbf{q}, \quad \mathbf{q}_s = \frac{\partial \mathbf{w}}{\partial t} \quad (11)$$

Under the combined action of mechanical load and pollutant concentration, the generalized Darcy's law of pore fluid can be expressed as [10]:

$$\begin{cases} q_x = (1-\omega)\left(-\frac{k_x}{\gamma_w} \frac{\partial u}{\partial x} + \omega \frac{k_x}{\gamma_w} \frac{RT}{M} \frac{\partial c}{\partial x}\right) \\ q_y = (1-\omega)\left(-\frac{k_y}{\gamma_w} \frac{\partial u}{\partial y} + \omega \frac{k_y}{\gamma_w} \frac{RT}{M} \frac{\partial c}{\partial y}\right) \\ q_z = (1-\omega)\left(-\frac{k_z}{\gamma_w} \frac{\partial u}{\partial z} + \omega \frac{k_z}{\gamma_w} \frac{RT}{M} \frac{\partial c}{\partial z}\right) \end{cases} \quad (12)$$

In the formula: ω represents the chemical permeability efficiency coefficient, R is the universal gas constant, γ_w is the specific gravity of water, T is the thermodynamic temperature, and k_x, k_y and k_z are the permeability coefficients in the x, y and z directions respectively. When the soil is an isotropic material, $k=k_x=k_y=k_z$ The hydraulic conductivity coefficient of the soil mass and the initial hydraulic conductivity coefficient satisfy [30].

$$k = k_0 \left(\frac{n}{n_0}\right)^3 \quad (13)$$

In the formula, k_0 represents the initial hydraulic conductivity coefficient.

Rowe et al. [31-33] found that when calculating the transportation of pollutants within the composite liner, the leakage of the geomembrane connected to the folds must be taken into account. Assuming that the width of the fold is much smaller than the length of the fold and the wetting radius of the leachate is the half-width of the fold, the volume leakage vector $\mathbf{Q}_{V,h}$ of the pollutant through the vulnerability and the fold can be expressed as [31, 32].

$$\mathbf{Q}_{V,h} = \frac{2h_d L_w}{l} \left[kb_w + \sqrt{kl\theta} \right] \quad (14)$$

In the formula: L_w represents the length of the connected folds, h_d is the head loss in the composite liner, l is the thickness of the clay cushion layer, k is the clay permeability coefficient tensor, $2b_w$ is the width of the folds, and θ is the water conductivity coefficient at the interface between the geomembrane and the clay cushion layer.

For the composite liner with a hole frequency of

m_h , the Darcy velocity vector caused by geomembrane leakage can be expressed as [34]

$$\mathbf{v}_a = \frac{m_h \mathbf{Q}_{V,h}}{A} \quad (15)$$

In the formula, A represents the area of the investigation area.

The Darcy velocity vector \mathbf{v}_a caused by the leakage of the geomembrane and the seepage velocity vector \mathbf{v}_c in the clay cushion layer are satisfied

$$\mathbf{v}_a = n\mathbf{v}_c \quad (16)$$

Substituting formula (16) into formula (12) yields

$$\begin{cases} q_x = (1-\omega)\left(-\frac{k}{\gamma_w} \frac{\partial u}{\partial x} + \omega \frac{k}{\gamma_w} \frac{RT}{M} \frac{\partial c}{\partial x} + v_{cx}\right) \\ q_y = (1-\omega)\left(-\frac{k}{\gamma_w} \frac{\partial u}{\partial y} + \omega \frac{k}{\gamma_w} \frac{RT}{M} \frac{\partial c}{\partial y} + v_{cy}\right) \\ q_z = (1-\omega)\left(-\frac{k}{\gamma_w} \frac{\partial u}{\partial z} + \omega \frac{k}{\gamma_w} \frac{RT}{M} \frac{\partial c}{\partial z} + v_{cz}\right) \end{cases} \quad (17)$$

Substituting formulas (10), (11) and (17) into formula (9) yields:

$$m_v \frac{\partial u}{\partial t} - m_c \frac{\partial c}{\partial t} + \nabla \cdot (\mathbf{q} + n \frac{\partial \mathbf{w}}{\partial t}) = 0 \quad (18)$$

2.4 Pollutant Transport Control equation

The mass conservation equation of pollutants in pore fluids can be expressed as

$$\frac{\partial(nc)}{\partial t} = -\nabla \mathbf{J}_f \pm Y \quad (19)$$

In the formula, Y represents the source and sink terms, and \mathbf{J}_f is the pollutant flux vector in the liquid phase, which can be written as

$$\mathbf{J}_f = \mathbf{J}_a + \mathbf{J}_m + \mathbf{J}_d = \mathbf{J}_a + \mathbf{J}_D \quad (20)$$

In the formula: \mathbf{J}_a represents the convective flux vector of the pollutant, \mathbf{J}_m represents the diffusing flux vector of the pollutant, \mathbf{J}_d represents the mechanical dispersive flux vector of the pollutant, and \mathbf{J}_D represents the hydrodynamic dispersive flux vector of the pollutant.

The convective diffusion flux vector of pollutants can be expressed as

$$\mathbf{J}_a = n\mathbf{q}c \quad (21)$$

The pollutant diffusion flux vector can be expressed as

$$\mathbf{J}_m = -n\mathbf{D}_m \nabla c \quad (22)$$

In the formula, \mathbf{D}_m represents the effective diffusion tensor of the solute in a porous medium and can be expressed as [35]

$$D_m = (1 - \omega)\tau D_0 \quad (23)$$

In the formula: D_0 is the diffusion coefficient of pollutants in open water bodies, τ is the curvature factor tensor of soil, $\tau = (\tau_x, \tau_y, \tau_z)^T = (n^m, n^m, n^m)^T$, m is an empirical parameter with a value of 2 [36].

The mechanical dispersion flux vector of pollutants can be expressed as

$$J_d = -nD_d \nabla c \quad (24)$$

In the formula, D_d is the mechanical diffusion coefficient tensor, which can be expressed as

$$D_d = -\alpha |q| \quad (25)$$

In the formula: α is the diffusion tensor, which can be written as $\alpha = (\alpha_T, \alpha_T, \alpha_L)^T$, where α_T is the transverse diffusion factor and α_L is the longitudinal diffusion factor. Hydrodynamic dispersion includes molecular diffusion and mechanical dispersion. Therefore, the hydrodynamic dispersion coefficient tensor can be written as

$$D = D_d + D_m \quad (26)$$

The vector of hydrodynamic dispersion flux of pollutants can be expressed as

$$J_D = nD \nabla c \quad (27)$$

$$\frac{\partial(nc)}{\partial t} + \frac{\partial [K_d(1-n)\rho_s c]}{\partial t} = \nabla(nD \cdot \nabla c - nqc) - \nabla \left[K_d(1-n)\rho_s c \frac{\partial w}{\partial t} \right] \pm Y \quad (32)$$

Equations (5), (18) and (33) together constitute the three-dimensional hydro-hydrochemical fully coupled pollutant transport equation, in which there are three variables: displacement vector w , super-porosity water pressure u and pollutant concentration c .

3. Numerical Calculation

In this section, relying on the established three-dimensional water-mechanical-chemical fully coupled model, the numerical calculation of the established model is carried out using the finite element software COMSOL Multiphysics.

Table 1. Model Parameters

parameter	Physical significance	short-cut process
D0/(m2 • s-1)	Diffusion coefficient of free water molecules	4.13 × 10-9
k0/(m • s-1)	Initial permeability coefficient	1 × 10-10
v	Poisson ratio	0.3
ω	Chemical permeability coefficient	0.02
n0	Initial porosity	0.5
kd/m3	adsorption coefficient	0.814 × 10-3
mv/(m • s2 • kg-1)	Coefficient of volume change caused by mechanical load	5 × 10-7
mc/(m-1 • s2 • kg-1)	Coefficient of volume change due to concentration	0.105 × 10-7

It can be obtained by substituting formulas (20), (21) and (27) into formula (19)

$$\frac{\partial(nc)}{\partial t} = -\nabla(nD \nabla c - nqc) \pm Y \quad (28)$$

The mass conservation equation of pollutants in the solid phase can be expressed as

$$\frac{\partial[(1-n)\rho_s S]}{\partial t} = -\nabla \cdot J_s \pm Y \quad (29)$$

In the formula, J_s is the flux vector of pollutants in the solid phase, and S is the mass of pollutants adsorbed by unit mass solid in soil particles.

When the adsorption of soil is linear isothermal adsorption, the mass of pollutants adsorbed per unit solid phase can be expressed as

$$S = K_d c \quad (30)$$

The flux vector J_s can be expressed as

$$J_s = (1-n)v_s \rho_s S \quad (31)$$

Substituting formulas (30) and (31) into formula (29) yields

$$\frac{\partial [K_d(1-n)\rho_s c]}{\partial t} = -\nabla \left[K_d(1-n)\rho_s c \frac{\partial w}{\partial t} \right] \pm Y \quad (32)$$

Assuming that the source terms are the same during adsorption and desorption, equations (28) and (32) are added to obtain the pollutant transport control equation

The size of the selected study area for numerical calculation is 4 m × 4 m × 1 m (Ω_1), and the model parameters are shown in Table 1. Based on the numerical calculation results, the changes in internal pore water pressure, soil deformation evolution and pollutant migration laws of the composite liner under two working conditions: the presence of holes in the geomembrane and the coexistence of wrinkles and holes were analyzed, and the coupling response laws of the two working conditions were compared and analyzed

$R/(J \cdot mol^{-1} \cdot K^{-1})$	Universal gas constant	8.314
$M/(kg \cdot mol^{-1})$	NaCl molar mass	0.0585
G/Pa	modulus of shearing	2.6×10^6
$\rho s/(kg \cdot m^{-3})$	density of solid particles	2.6×10^3
$\rho w/(kg \cdot m^{-3})$	Pore fluid density	1×10^3
$\alpha L/m$	Longitudinal diffuseness	0.001
$\alpha T/m$	Horizontal dispersion	0.01
Lws/m	Fold length	500
A/m^2	Size of the study area	10000
mh	Distribution density of holes on geomembranes	2.5
$\theta/(m \cdot s^{-2})$	Water conductivity at the interface between geotextile membrane and clay cushion	2×10^{-10}

Note: The values of each parameter in Table 1 are the same as those in literature [37-39]

3.1 Study on the Coupling Response Law of Hydraulicization of the Underlying Clay Cushion under the Influence of Leakage

3.1.1 Boundary Conditions

The idealized model and discrete model of the composite liner when the geomembrane is in a leak are shown in Figure 1 and Figure 2. It can be seen from Figure 1 and Figure 2 that the leachate can only be transmitted downward through the circular area with a radius of 0.1m (Ω_2) under this condition, and the parameters used in numerical calculation are shown in Table 1.

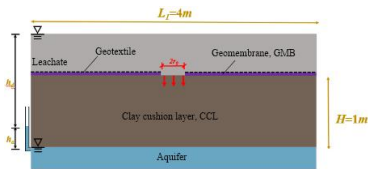


Figure 1. Idealized Model Corresponding to the First Working Condition

3.1.2 Variation Law of Pore Water Pressure

Figure 3 shows the pore water pressure distribution cloud inside the cushion at different times when the geomembrane is leaking. It can be seen from Figure 3 (a)-(d) that in the initial stage (0.1 year), near the leakage area, the positive pore water pressure spreads throughout the soil layer. About one year later, the positive pore water pressure completely dissipates, and only the negative pore water pressure exists inside the cushion layer. However, as time goes by, the negative pore pressure around the leakage area begins to gradually dissipate. The reason for the above phenomenon is that mechanical consolidation dominates in the initial stage, and the pore water pressure is mainly caused by mechanical loads. About one year later, the mechanical consolidation is basically

Initial condition:

$$w(x, y, z, 0) = 0 \text{ m}, u(x, y, z, 0) = 0 \text{ kPa}, c(x, y, z, 0) = 0 \text{ kg/m}^3 \quad (0 < x < L_1, 0 < y < L_1, 0 < z < H)$$

Boundary condition:

$$w(x, y, H, t) = 0 \text{ m}, w(0, y, z, t) = w(L_1, y, z, t) = 0 \text{ m}, w(x, y, H, t) = 0 \text{ m};$$

$$u(x, y, 0, t) = u(x, y, H, t) = 0 \text{ kPa}, u(0, y, z, t) = u(L_1, y, z, t) = \partial u / \partial x = 0 \text{ kPa/m}, u(x, 0, z, t) = u(x, L_1, z, t) = \partial u / \partial y = 0 \text{ kPa/m};$$

$$c(x, y, 0, t) = 58.5 \text{ kg/m}^3 \quad ((x, y, 0) \in \Omega_2), c(x, y, 0, t) = 0 \text{ kg/m}^3 \quad ((x, y, 0) \notin \Omega_2), c(x, y, H) = 0 \text{ kg/m}^3, c(0, y, z, t) = c(L_1, y, z, t) = \partial c / \partial x = 0 \text{ kg/m}^4, c(x, 0, z, t) = c(x, L_1, z, t) = \partial c / \partial y = \partial c / \partial x = 0 \text{ kg/m}^4 \quad (t \geq 0).$$

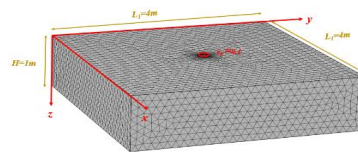


Figure 2. Discrete Model Corresponding to the First Working Condition

completed, and the chemoosmotic consolidation begins to dominate. At this time, the pore water pressure is mainly caused by the chemical osmotic pressure, that is, the suction force, so the pore water pressure shows a negative value. Since geomembranes can prevent the leakage of leachate, pollutants can only be transferred to the interior of the soil through the leakage area. Therefore, chemical osmotic consolidation and negative pore water pressure mainly occur around the leakage area. However, with the migration of pollutants, the concentration gradient of pollutants inside and outside the soil mass decreases, and the chemical osmotic pressure on the soil mass decreases. Meanwhile, with the completion of chemically-osmotic consolidation and the drainage of pore water, the negative pore water pressure begins to decay

rapidly.

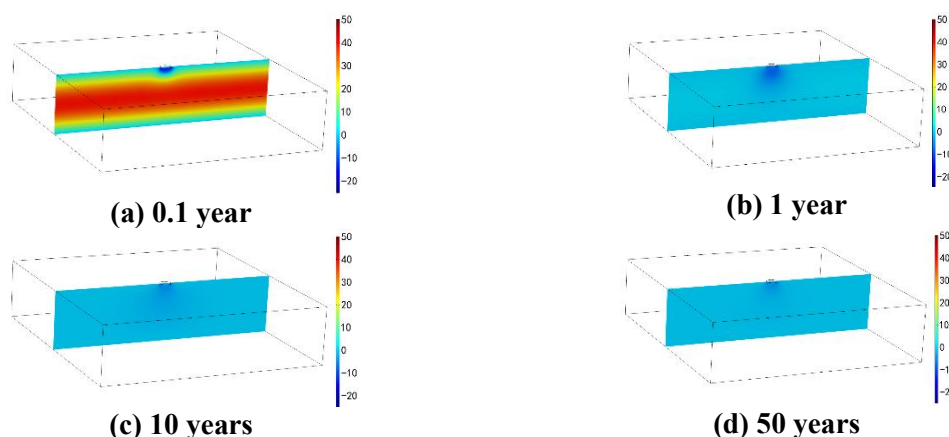


Figure 3. Nephogram of Pore Water Pressure Variation in the Underlying Clay Liner at Different Times

3.1.3 Evolution Law of Settlement of Underlying Clay Cushion

Figure 4 shows the evolution of clay cushion settlement when there is a leak in geotextile membrane at 0.1 year, 1.0 year, 10 years and 50 years. It can be seen from Figure 4 (a)-(d) that in the initial stage, the soil settlement gradually increases, reaches stability in about one year, and then remains basically unchanged. This is mainly because the positive pore water pressure caused by mechanical loads in the initial stage

gradually dissipates, and the mechanical consolidation of the soil mass gradually completes. In addition, it can be observed from the figure that the settlement amount of the underlying layer beneath the leakage area is larger than that of the surrounding soil. This is mainly because pollutants can be transmitted into the soil through the leakage area, inducing chemically-permeable consolidation in the soil and increasing the settlement amount of the soil.

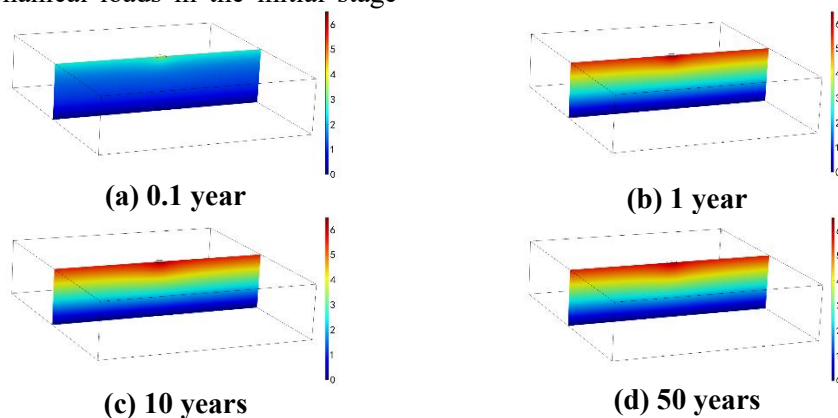


Figure 4. Nephogram of Clay Liner Settlement Variation at Different Times

3.1.4 Distribution Law of Pollutant Concentration in Subgrade

Figure 5 shows the distribution of pollutant concentration in the subgrade when the geomembrane is leaking at different times. As can be seen from Figures 5 (a)-(d), the presence of the geomembrane completely hinders the migration of pollutants, allowing the pollutants to be transmitted only through the circular leakage area and the downward cushion layer. However, since the direction in which pollutants are transmitted from the circular leakage area to the interior of the cushion layer is not unique, the migration rate of pollutants in each direction

is significantly weakened, and the pollutants are mainly concentrated in the upper part of the cushion layer. Furthermore, by comparing the cloud maps of pollutant concentration distribution over 0.1 years, 1 year, 10 years and 50 years, it can be seen that the changes in pollutant concentration distribution in the initial stage (0.1-1 year) are more significant than those in the later stage (10-50 years). This is mainly because the convective effect caused by the mechanical load in the initial stage can accelerate the migration of pollutants into the interior of the cushion layer to a certain extent.

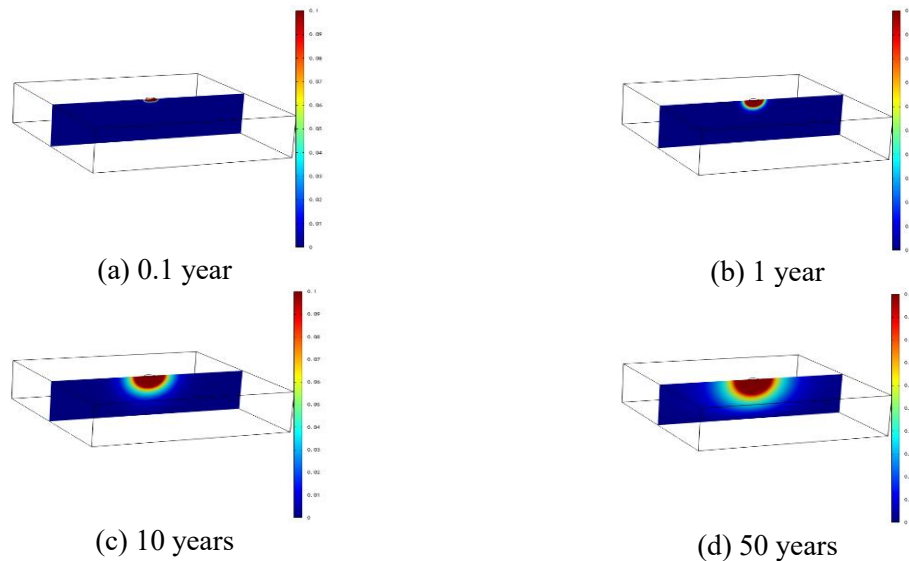


Figure 5. Nephogram of Pollutants Distribution in the Underlying Clay Liner at Different Times

3.2 Study on the Coupling Response Law of Hydraulicization of Underlying Clay Cushion under the Influence of Faults and Folds

3.2.1 Boundary Conditions

The contact conditions between the geomembrane and the clay cushion layer are affected by the compaction degree and surface flatness of the horizontal clay cushion layer. When the geomembrane is exposed to direct sunlight during construction and the horizontal clay layer is not fully compacted with an uneven surface, there will be many wrinkles on the geomembrane. Meanwhile, due to the high tensile strain at the folds of the geomembrane, holes often appear above it. Therefore, this section conducts numerical calculations for the working conditions where both vulnerabilities and wrinkles exist simultaneously. The idealized model and discretized model corresponding to this working condition are shown in Figures 6

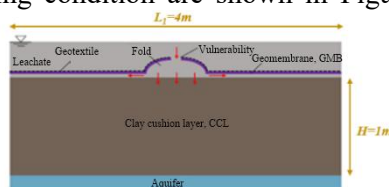


Figure 6. Idealized Model Corresponding to the Second Working Condition

3.2.2 Variation Law of Pore Water Pressure

Figure 8 shows the pore water pressure distribution cloud of x-z and y-z at the center point of the fold in 0.1 year, 1.0 year, 10 years and 50 years.

It can be seen from Figure 8 (a) that at the shallower depth directly beneath the folds (on

and 7 respectively. It can be seen from the idealized model and the discretization model that the circular leakage area is connected to the folds with a half-width of 0.2 m. The locations of the vulnerabilities and folds are defined as the area Ω_3 . The parameters used for numerical calculation are shown in Table 1.

Initial condition:

$$w(x, y, z, 0)=0 \text{ m}, u(x, y, z,0)=0 \text{ kPa}, c(x, y, z,0)=0 \text{ kg/m}^3 (0<x<L_1, 0<y<L_1, 0<z<H)$$

Boundary condition:

$$w(x, y, H, t) = 0 \text{ m}, w(0, y, z, t) = w(L_1, y, z, t) = 0 \text{ m}, w(x, y, H, t) = 0 \text{ m};$$

$$u(x, y, 0, t) = u(x, y, H, t)=0 \text{ kPa}, u(0, y, z, t) = u(L_1, y, z, t) = \partial u/\partial x=0 \text{ kPa/m}, u(x, 0, z, t) = u(x, L_1, z, t) = \partial u/\partial y=0 \text{ kPa/m};$$

$$c(x, y, 0, t) = 58.5 \text{ kg/m}^3 ((x, y, 0) \in \Omega_3), c(x, y, 0, t) = 0 \text{ kg/m}^3 ((x, y, 0) \notin \Omega_3), c(x, y, H) = 0 \text{ kg/m}^3, c(0, y, z, t) = c(L_1, y, z, t) = \partial c/\partial x=0 \text{ kg/m}^4, c(x, 0, z, t) = c(x, L_1, z, t) = \partial c/\partial y = \partial c/\partial x=0 \text{ kg/m}^4 (t \geq 0).$$

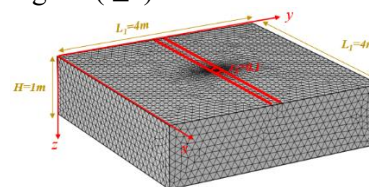


Figure 7. Discrete Model Corresponding to the Second Working Condition

the x-z section), due to the high concentration of pollutants, the chemoosmotic consolidation of the soil is intense, and the pore water pressure shows negative. While at the deeper depth, due to the influence of mechanical loads, the pore water pressure shows positive. Meanwhile, as can be seen from Figures 8 (b)-(d), in the later

stage of the simulation (more than one year), the positive pore water pressure completely dissipated, and the pore water pressure below the folds completely turned negative. However, with the transportation of pollutants and the discharge of pore water, the negative pore water pressure gradually dissipated. Furthermore, the distribution law of negative pore water pressure on the y - z section passing through the center

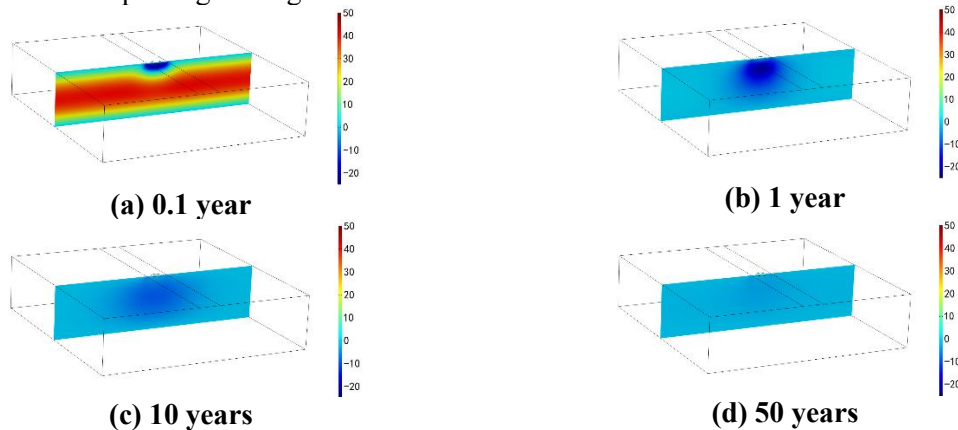


Figure 8. Nephogram of Pore Water Pressure Variation in the Underlying

3.2.3 Evolution Law of Settlement of Underlying Clay Cushion

Figure 9 shows the cloud maps of the soil settlement evolution laws of the x - z and y - z sections passing through the center point of the fold at different times. It can be seen that the soil settlement gradually increases over time, reaching the maximum in about one year, and then begins to rebound. This is mainly because the mechanical consolidation plays a dominant role in the initial stage. As the mechanical consolidation is completed, the soil settlement gradually increases. About one year after the mechanical consolidation is completed, the soil settlement reaches its peak. Subsequently, the chemoosmotic consolidation process began to control the soil deformation. However, with the transport of pollutants, the concentration difference of pollutants inside and outside the cushion layer decreased, the chemical osmotic pressure on the soil decreased, and the degree of chemoosmotic consolidation weakened. Therefore, the soil settlement showed a rebound. Furthermore, it can be seen from Figure 9 that when the soil depth is the same, there are significant differences in soil settlement at each position of the y - z section (perpendicular to the fold direction), specifically manifested as higher settlement in the area where the fold is located than in the area without the fold. This is mainly because in areas with fewer folds,

point of the fold (perpendicular to the direction of the fold) is the same as that when there are only loopholes, but the influence range is significantly expanded. This is mainly because the folds on the geomembrane will increase the leakage range of pollutants and enhance the influence of chemical reactions on the pore water pressure.

chemical-permeation consolidation occurs in the soil beneath the folds, increasing the settlement deformation of the soil. The difference in settlement amount between the area where the wrinkles are located and the area without wrinkles will cause uneven settlement of the upper soil of the cushion layer. The uneven settlement of the soil will further increase the area of the leakage zone, thus forming a vicious cycle.

3.2.4 Distribution Law of Pollutant Concentration in Subgrade

Figure 10 shows the cloud maps of pollutant concentration distribution at the x - z and y - z cross-sections passing through the center point of the folds at 0.1 years, 1 year, 10 years and 50 years. It can be seen from the figure that the x - z cross-section is parallel to the direction of the folds, and the pollutants will be uniformly transmitted downward through the folds. The y - z section is perpendicular to the direction of the folds. Pollutants will not only be transmitted downward through the folds but also diffuse to the areas without folds. This is mainly because there are differences in pollutant concentrations perpendicular to the direction of the folds. Driven by the concentration differences, pollutants will diffuse to the areas without folds. Furthermore, it can be seen from the figure that the cloud map of the pollutant concentration distribution in the y - z section passing through

the center point of the fold, that is, in the direction perpendicular to the fold, is similar to the cloud map of the pollutant concentration distribution when only the vulnerability exists. However, the pollutant migration rate

considering the influence of the fold is significantly accelerated. This is mainly because the fold will increase the leakage range of the pollutant and accelerate the transportation rate of the pollutant.

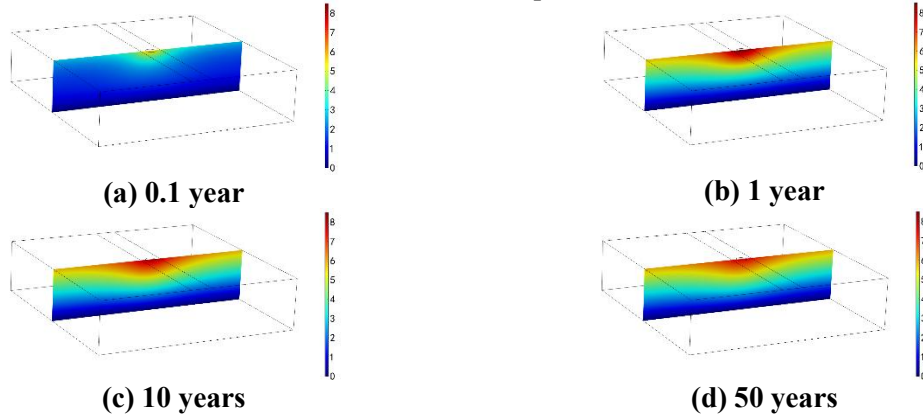


Figure 9. Nephogram of Clay Liner Settlement at Different Cross Sections and Times

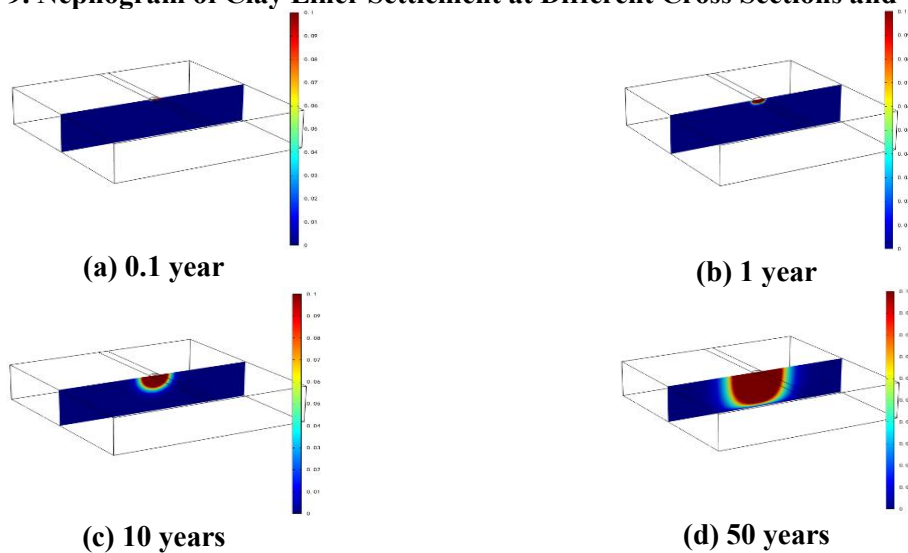


Figure 10. Nephogram of Pollutants Distribution in the Underlying Clay Liner at Different Cross Sections and Times

3.3 Comparison of the Two Working Conditions

This section studies the influence of wrinkles on the water-mechanochemical coupling process of the horizontal clay cushion layer under the composite liner by comparing the changes in pore water pressure, soil settlement evolution and pollutant transport differences at the centerline position of the two working conditions of not considering and considering wrinkles.

3.3.1 Comparison Results of Pore Water Pressure Changes

Figure 11 presents the comparison results of the variation laws of pore water pressure under two working conditions. It can be seen from the

figure that the negative pore water pressure corresponding to working condition two is higher than that of working condition one. Furthermore, unlike in condition one where the negative pore water pressure is mainly maintained at the upper part of the cushion layer, in condition two, the negative pore water pressure will extend into the soil interior, and the dissipation rate will increase significantly. This is mainly because the negative pore water pressure is mainly caused by chemically-permeable consolidation. When there are wrinkles in the geomembrane, the migration rate of pollutants increases significantly, and the chemically-permeable consolidation path of the soil is high. Meanwhile, due to the fast migration rate of pollutants corresponding to

working condition two, the accumulation concentration of pollutants within the cushion layer is high, and the concentration gradient of pollutants inside and outside the soil decreases rapidly. Therefore, the chemical osmotic pressure on the soil decreases strongly, and the corresponding negative pore water pressure dissipates rapidly.

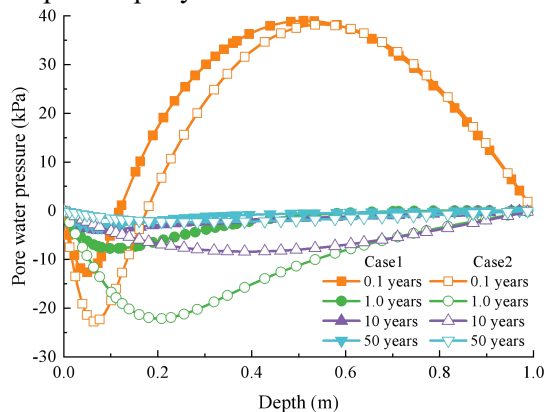


Figure 11. Comparison of Pore Water Pressure under Different Operating Conditions

3.3.2 Comparison Results of Sedimentation Volume Evolution

Figure 12 shows the comparison results of the soil settlement evolution laws under two working conditions. It can be seen from Figure 12 that when the simulation time is the same, the soil settlement corresponding to condition two is greater than that of condition one. This is mainly caused by the fact that during the same period of time, when considering the influence of folds, the pollutant transport rate is fast and the degree of chemically-permeable consolidation of the soil mass is high. Furthermore, it can also be seen that when the influence of folds is not considered, the soil settlement amount will first increase and then remain stable. When considering the influence of folds, the soil settlement evolution is mainly divided into two stages: (I) the ascending stage, (II) the rebound stage. From the above analysis, it can be known that the increase in soil settlement is mainly caused by mechanical consolidation, while the rebound stage of settlement is mainly related to chemical-osmotic consolidation. The degree of chemopermeation consolidation is controlled by the concentration difference inside and outside the soil [41]. However, due to the existence of folds, the migration rate of pollutants increases significantly, the accumulated concentration inside the cushion layer increases greatly, the concentration difference inside and outside the

soil decreases sharply, the chemical permeation load decreases significantly, and the degree of chemopermeation consolidation is greatly weakened. Therefore, obvious rebound occurs in soil settlement.

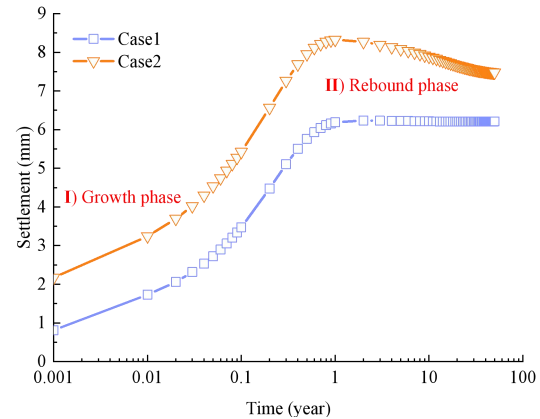


Figure 12. Comparison of Soil Settlement Evolution under Different Operating Conditions

3.3.3 Comparison Results of Pollutant Distribution

Figure 13 presents the comparison results of pollutant migration laws under two working conditions. It can be clearly seen from Figure 13 that at the same time and depth, the pollutant migration rate corresponding to working condition two is faster than that of working condition one. Moreover, as time goes on, the difference in pollutant accumulation concentrations between the two working conditions gradually increases, which is manifested in the figure as the curve spacing corresponding to the two working conditions gradually increasing. This is mainly because the leakage area corresponding to working condition one is small. Pollutants will spread in all directions through the circular leakage area, thereby significantly weakening the vertical migration rate of pollutants.

When the relative concentration of pollutants at a certain position inside the cushion layer reaches 0.1, it is considered that this position has been punctured by pollutants [40]. Based on this, the pollutant breakdown line is drawn. It is found that when the simulation time is 50 years, the pollutant breakdown depth corresponding to working condition one is 0.41 m, and the pollutant breakdown depth corresponding to working condition two is 0.81 m. The breakdown depth of the two working conditions differs by 0.40 meters. It can be seen from this that when there are only loopholes on the geomembrane, the migration rate of pollutants is

slow, the penetration depth of pollutants is relatively shallow, and they are mainly concentrated in the upper part of the cushion layer. When wrinkles exist simultaneously on the geomembrane, the migration rate of pollutants is significantly accelerated and the penetration depth is greatly increased. The research finds that the compaction and flatness of the underlying cushion layer and the direct sunlight conditions will directly affect the number of wrinkles on the geomembrane. Therefore, during the construction of geomembrane, it is necessary to ensure that the surface of the clay layer is as flat as possible and minimize direct sunlight. This will effectively reduce the number of wrinkles on the geomembrane and extend the service life and lifespan of the landfill.

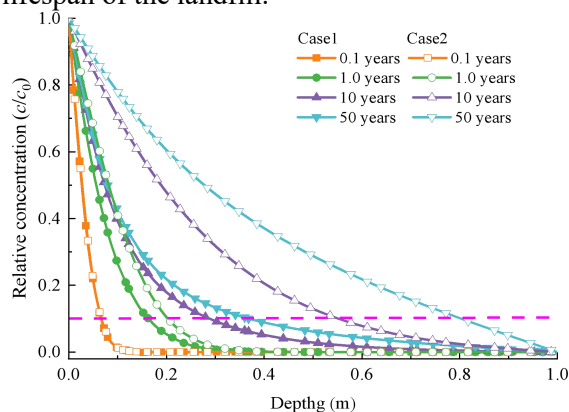


Figure 13. Comparison of Pollutant Migration and Distribution under Different Operating Conditions

4. Conclusion

When there are defects in the geomembrane, due to the leakage of pollutants, the underlying clay cushion layer will undergo chemically-permeable consolidation, resulting in negative pore water pressure within the soil.

When there are only holes on the geomembrane, the soil settlement first increases and then remains stable. However, when the geomembrane has both holes and wrinkles at the same time, the soil settlement evolution is mainly divided into two stages: the growth stage I and the rebound stage II. In addition, the wrinkles on the geomembrane will cause uneven settlement of the underlying soil, thereby further increasing the leakage area of the geomembrane. When there are only loopholes on the geomembrane, the migration of pollutants is slow and mainly concentrated in the upper part of the cushion layer. When there are both holes

and wrinkles on the geomembrane at the same time, the migration rate of pollutants increases significantly, and the penetration depth of pollutants extends rapidly downward. When the simulation time is 50 years, compared with the working condition where only vulnerabilities exist and both vulnerabilities and wrinkles exist simultaneously, the pollutant breakdown depth increases by 0.4 meters.

During the construction of geomembrane, direct sunlight should be avoided as much as possible to ensure the surface of the horizontal clay cushion layer is as flat as possible, thereby reducing the number of wrinkles on the geomembrane and improving the anti-seepage and anti-fouling performance of the composite liner.

References

- [1] Chen Yunmin, Xie Haijian, Zhang Chunhua. Review on penetration of barriers by contaminants and technologies for groundwater and soil contamination control [J]. *Advances in Science and Technology of Water Resources*, 2016, 36(01): 1-10.
- [2] Huang L, Zhao C G, Liu Y, et al. 3D contaminant migration model with consolidation dependent transport coefficients [J]. *Acta Mechanica Sinica*, 2012, 28(1): 151-163.
- [3] Chen Y M. A fundamental theory of environmental geotechnics and its application [J]. *Chinese Journal of Geotechnical Engineering*, 2014, 36(1): 1-46.
- [4] Zhou Lian, An Da, Yang Yanmei, et al. Predicting leakage and contaminant transport through composite liners in hazardous waste landfill [J]. *Acta Scientiae Circumstantiae*, 2017, 37(06): 2210-2217.
- [5] Zhang Qian, Lu Hai-jun, Cai Guang-hua, et al. Adsorption and transportation properties of cadmium in modified clay containing sewage sludge ash as landfill liner [J]. *Journal of Southeast University (Natural Science Edition)*, 2016, 46 (z1): 174-178.
- [6] Li Y C, Cleall P J, Thomas H R. Multi-dimensional chemo-osmotic consolidation of clays [J]. *Computers and Geotechnics*, 2011, 38(4): 423-429.
- [7] Kooi H, Garavito A M, Bader S. Numerical modelling of chemical osmosis and ultrafiltration across clay formations [J]. *Journal of Geochemical Exploration*, 2003,

- 78: 333-336.
- [8] Ferrell R E, Aagaard P, Forsman J, et al. Application of a geochemical transport model to predict heavy metal retention (Pb) by clay liners [J]. *Applied Clay Science*, 2002, 21 (1-2): 59-66.
- [9] Li Z, Alessi D, Zhang P, et al. Organo-illite as a low permeability sorbent to retard migration of anionic contaminants [J]. *Journal of Environmental Engineering*, 2002, 128(7): 583-587.
- [10] Baderr S, Kooi H. Modelling of solute and water transport in semi-permeable clay membranes: comparison with experiments [J]. *Advances in Water Resources*, 2005, 28(3): 203-214.
- [11] Zhang Z H, Masum S A, Thomas H R, et al. Modeling fully coupled hydraulic-mechanical-chemical processes in a natural clay liner under mechanical and chemico-osmotic consolidation [J]. *Environmental Science and Pollution Research*, 2018, 25(36): 36173-36183.
- [12] Zheng X, Wang L, Xu Y. Analytical solutions of 1-D chemo-hydro-mechanical coupled model of saturated soil considering osmotic efficiency [J]. *International Journal for Numerical and Analytical Methods in Geomechanics*, 2021, 45(17): 2522-2540.
- [13] Smith D W. One-dimensional contaminant transport through a deforming porous medium: theory and a solution for a quasi-steady-state problem [J]. *International journal for numerical and analytical methods in geomechanics*, 2000, 24(8): 693-722.
- [14] Qiu J W, Chen X L, Tong J. Fully transient analytical solution for solute transport in 1D deforming saturated porous media considering nonlinear compressibility and permeability [J]. *Applied Mathematical Modelling*, 2022, 108, 122-141.
- [15] Xie H J, Yan H X, Feng S J, et al. An analytical model for contaminant transport in landfill composite liners considering coupled effect of consolidation, diffusion, and degradation [J]. *Environmental Science and Pollution Research*, 2016, 23 (19): 19362-19375.
- [16] Kaczmarek M, Hueckel T, Chawla V, et al. Transport through a clay barrier with the contaminant concentration dependent permeability [J]. *Transport in porous media*, 1997, 29(2): 159-178.
- [17] Peters G P, Smith D W. The influence of advective transport on coupled chemical and mechanical consolidation of clays [J]. *Mechanics of Materials*, 2004, 36(5): 467-486.
- [18] Tian Gailei, Zhang Zhihong. Analysis on soil consolidation deformation and solute transport under non-isothermal conditions [J]. *Journal of Southeast University (Natural Science Edition)*, 2021, 51(5): 819-825.
- [19] Zhang Z H, Fang Y F. A Three-Dimensional Model Coupled Mechanical Consolidation and Contaminant Transport [J]. *Journal of Residuals Science & Technology*, 2016, 13(2): 121-133.
- [20] Zhang Z H, Fang Y F, Li X D. 3D transport of solute in deformable soils with different adsorption modes [J]. *Soil Mechanics and Foundation Engineering*, 2017, 54(2): 128-136.
- [21] Bouazza A. Geosynthetic clay liners [J]. *Geotextiles and Geomembranes*, 2002, 20(1): 3-17.
- [22] Rowe R K, Brachman R W I. Assessment of equivalence of composite liners [J]. *Geosynthetics International*, 2004, 11(4): 273-286.
- [23] Yan H, WU J, Thomas H R, et al. Analytical model for coupled consolidation and diffusion of organic contaminant transport in triple landfill liners [J]. *Geotextiles and Geomembranes*, 2021, 49(2): 489-499.
- [24] Fan J, Rowe R K. Effect of a lateral drainage layer on leakage through a defect in a geomembrane overlain by saturated tailings [J]. *Geotextiles and Geomembranes*, 2024, 52(4): 383-395.
- [25] Take W A, Chappel M J, Brachman R W I, et al. Quantifying geomembrane wrinkles using aerial photography and digital image processing [J]. *Geosynthetics International*, 2007, 14(4): 219-227.
- [26] Giroud J P. Quantification of geosynthetic behavior [J]. *Geosynthetics International*, 2005, 12(1): 2-27.
- [27] Rowe R K. Long-term performance of contaminant barrier systems [J]. *Geotechnique*, 2005, 55(9): 631-678.
- [28] Zhan T L T, Guan C, Xie H J, et al. Vertical migration of leachate pollutants in clayey soils beneath an uncontrolled landfill at Huainan, China: a field and theoretical investigation [J]. *Science of the Total Environment*, 2014, 470-471: 290-298.

- [29] Zhang Zhihong, Shi Yumin, Zhu Min. Coupled hydro-mechanical-chemical model for clay liner [J]. Chinese Journal of Geotechnical Engineering, 2016, 38(7): 1283-1290.
- [30] Hart R D, St John C M. Formulation of a fully coupled thermal-mechanical-fluid flow model for non-linear geologic systems [J]. International Journal of Rock Mechanics and Mining Science and Geomechanics Abstracts, 1986, 23(3): 213-224.
- [31] Rowe R K. Geosynthetics and the minimization of contaminant migration through barrier systems beneath solid waste [J]. 1998: 27-103.
- [32] Rowe R K, Chappel M J, Brachman R W I, et al. Field study of wrinkles in a geomembrane at a composite liner test site [J]. Canadian Geotechnical Journal, 2012, 49 (10): 1196-1211.
- [33] Rowe R K. Protecting the environment with geosynthetics: 53rd Karl Terzaghi lecture [J]. Journal of Geotechnical and Geoenvironmental Engineering, 2020, 146(9): 040200.
- [34] Xie H J, Chen Y M, Lou Z H. An analytical solution to contaminant transport through composite liners with geomembrane defects [J]. Science China Technological Sciences, 2010, 53(5): 1424-1433.
- [35] Malusis M A, Kang J B, Shackelford C D. Restricted salt diffusion in a geosynthetic clay liner [J]. Environmental Geotechnics, 2015, 2(2): 68-77.
- [36] Liu Jianguo, Wang Hongtao, Nie Yong-feng. Fractal model for predicting effective diffusion coefficient of solute in porous media [J]. Advances in Water Science, 2004, 15 (04): 458-462.
- [37] Rowe R K. Short and long-term leakage through composite liners [J]. Canadian Geotechnical Journal, 2012b, 49(2): 141-169.
- [38] Zhang Chunhua, Huang Jiangdong, Deng Zhengding, et al. One-dimension model for transport of organic contaminants in double-artificial composite liner under thermal osmosis [J]. Chinese Journal of Geotechnical Engineering, 2024, 46(06): 1254-1262.
- [39] Zhang Z H, Masum S A, Thomas R H, et al. Modeling fully coupled hydraulic-mechanical-chemical processes in a natural clay liner under mechanical and chemico-osmotic consolidation [J]. Environmental science and pollution research international, 2018, 25 (36): 36173-36183.
- [40] Zhang Chunhua, Wu Jiawei, Chen Yun, et al. Simplified method for determination of thickness of composite liners based on contaminant breakthrough time [J]. Chinese Journal of Geotechnical Engineering, 2020, 42(10): 1841-1848.
- [41] Zhang Zhihong, Shi Yumin. Influence mechanism and calculation method for soil deformation under double load [J]. Journal of Southeast University (Natural Science Edition), 2016, 46(S1): 148-152.